PHOTONICS Research

Exceptional points and enhanced nanoscale sensing with a plasmon-exciton hybrid system

Hong Jiang,[1] Weidong Zhang,[1] Guowei Lu,[1,2,3,6] Lulu Ye,[1] Hai Lin,[1] Jinglin Tang,[1] Zhaohang Xue,[1] Zheng Li,[1,2,3,7] Haitan Xu,[4,5,8] and Qihuang Gong[1,2,3]

[1]State Key Laboratory for Mesoscopic Physics, Collaborative Innovation Center of Quantum Matter, Nano-optoelectronics Frontier Center of the Ministry of Education, School of Physics, Peking University, Beijing 100871, China
[2]Collaborative Innovation Center of Extreme Optics, Shanxi University, Taiyuan 030006, China
[3]Peking University Yangtze Delta Institute of Optoelectronics, Nantong 226010, China
[4]Shenzhen Institute for Quantum Science and Engineering, Southern University of Science and Technology, Shenzhen 518055, China
[5]School of Physical Sciences, University of Science and Technology of China, Hefei 230026, China
[6]e-mail: guowei.lu@pku.edu.cn
[7]e-mail: zheng.li@pku.edu.cn
[8]e-mail: xuht@sustech.edu.cn

Received 15 October 2021; revised 3 December 2021; accepted 19 December 2021; posted 21 December 2021 (Doc. ID 445855); published 1 February 2022

Singularities in the spectra of open systems, known as exceptional points (EPs), have been shown to exhibit nontrivial topological properties and enhanced sensitivities. Here, we propose a novel approach to realize the EPs in a plasmon-exciton hybrid system and explore their applications in enhanced nanoscale sensing technology. We consider a plasmon-exciton system composed of a gold nanorod and a monolayer WSe_2. By controlling the geometric parameters of the nano-hybrid system, we obtain simultaneous coalescence of the resonance frequencies and loss rates of the hybrid system, which is a unique feature of EPs. Numerical simulations show its application in enhanced nanoscale sensing for environmental refractive indices. Our work opens the way to a new class of sensors based on EP-enhanced sensing, with intrinsic nanoscale sensitivity due to the sub-diffraction-limit size of the plasmon-exciton nano-hybrid system.

https://doi.org/10.1364/PRJ.445855

1. INTRODUCTION

Exceptional points (EPs) in non-Hermitian systems have attracted broad interest in recent years due to their topological properties and applications in sensing technology [1–4]. The energy eigenvalues of non-Hermitian systems coalesce at the EPs [5], and the complex eigenspectra possess the topology of complex Riemann surfaces. EPs exist in various physical systems, including microwave [6,7], photonic [8–27], optomechanical [28,29], atomic [30,31], electronic [32–35], condensed matter [36,37], acoustic [38], and other systems [39–41]. The nontrivial topological property of EPs makes the spectra of non-Hermitian systems fundamentally different from those of Hermitian systems [42–50]. Topological dynamics by adiabatic encircling of EPs has recently been realized in optomechanical experiments [28,51], which can be simulated by microwave and optical waveguide systems [52–57]. On the other hand, the nonlinear signature of the complex spectra around the EP singularities has been used for advanced sensing technology with EP-enhanced sensitivity [13,14,20,27,35,58]. So far, EP-enhanced sensing has mainly been focused on systems above the optical wavelength scale due to diffraction limits. Local surface plasmon-exciton hybrid systems can offer sensing devices beyond the diffraction limit and with intrinsic nanoscale spatial resolution [59–62]. It is intriguing to develop a scheme to implement the EPs in plasmon-exciton systems for enhanced sensitivity while maintaining the advantages that plasmon-exciton sensors already possess.

Here, we propose an experimental scheme to realize EPs in a plasmon-exciton hybrid system that consists of a gold nanorod (GNR) and monolayer WSe_2. By tuning the geometric parameters of the hybrid system, we observe an EP in the complex eigenspectrum. We then apply the plasmon-exciton system operating near the EP to sense the variation of environmental refractive indices, and demonstrate significantly enhanced nanoscale sensitivity by numerical experiments.

2. THEORY AND CONFIGURATIONS

Our plasmon-exciton hybrid system is depicted in Fig. 1(a). A monolayer of WSe_2 is placed on a glass substrate and coated with a thin layer of HfO_2. A GNR is then placed on top of HfO_2. The GNR diameter is 30 nm, with variable lengths

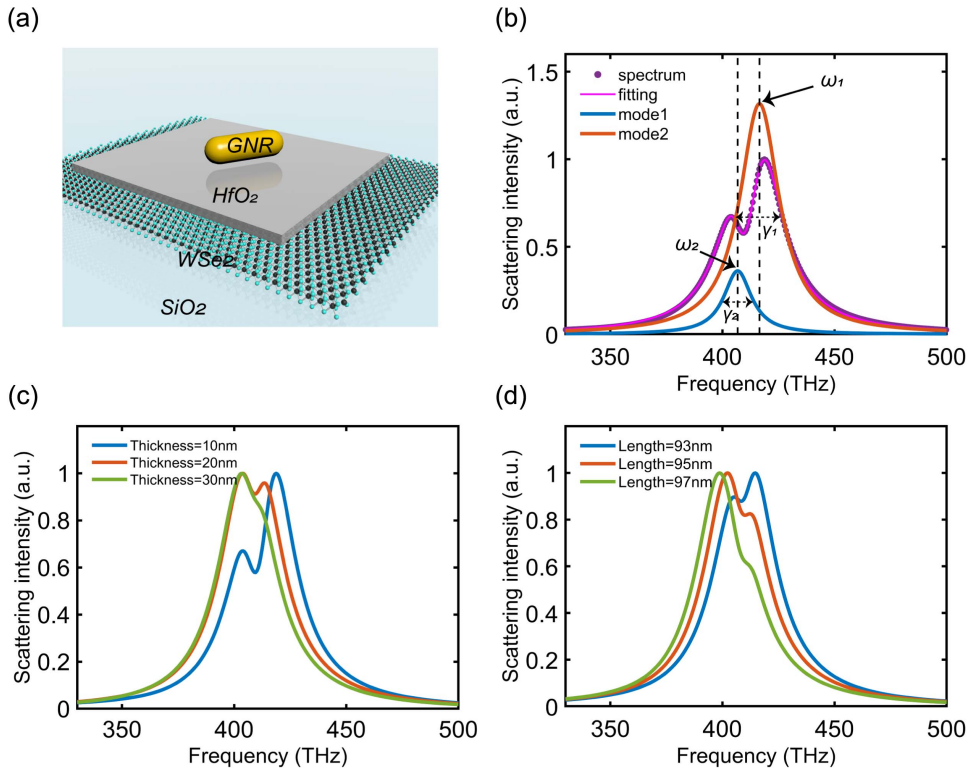

Fig. 1. Plasmon-exciton system with adjustable scattering spectrum. (a) Schematic of the plasmon-exciton system composed of a GNR and a monolayer WSe_2 separated by an auxiliary layer of HfO_2. (b) Scattering spectrum of the plasmon-exciton system. The purple points correspond to the scattering spectrum from numerical simulation, with a HfO_2 thickness of 10 nm and a GNR length of 94 nm. The red curve is the double-Lorentzian fitting result of the scattering spectrum. Blue and green curves are the individual hybrid modes extracted from the fitting result. (c) Scattering spectra for various thicknesses (10 nm, 20 nm, and 30 nm) of HfO_2 with GNR length of 94 nm. (d) Scattering spectra for various lengths (93 nm, 95 nm, and 97 nm) of GNR with HfO_2 thickness of 20 nm.

around 100 nm. The size of the monolayer WSe_2 is set as 5 μm × 10 μm, so it is much larger than the size of the GNR. The interaction between the longitudinal plasmon mode of GNR and the exciton mode of WSe_2 leads to two hybrid modes. We can describe the plasmon-exciton hybrid system with the coupled mode equation:

$$\frac{\mathrm{d}}{\mathrm{d}t}\begin{pmatrix} a_1 \\ a_2 \end{pmatrix} = -i\begin{pmatrix} \omega_1 - i\frac{\gamma_1}{2} & g \\ g & \omega_2 - i\frac{\gamma_2}{2} \end{pmatrix}\begin{pmatrix} a_1 \\ a_2 \end{pmatrix}, \quad (1)$$

where $\omega_{1,2}$ and $\gamma_{1,2}$ are the resonance frequencies and loss rates of the plasmon and exciton modes, and g is the coupling coefficient. The complex energy eigenvalues of the coupled system are given by

$$\omega = \omega_{\mathrm{ave}} - i\gamma_{\mathrm{ave}} \pm \sqrt{g^2 + \left(\omega_{\mathrm{diff}} + i\frac{\gamma_{\mathrm{diff}}}{2}\right)^2}, \quad (2)$$

where $\omega_{\mathrm{ave}} = \frac{\omega_1+\omega_2}{2}$ and $\gamma_{\mathrm{ave}} = \frac{\gamma_1+\gamma_2}{2}$ are the average values of resonance frequencies and loss rates of the uncoupled plasmon and exciton modes, while $\omega_{\mathrm{diff}} = \frac{\omega_1-\omega_2}{2}$ and $\gamma_{\mathrm{diff}} = \frac{\gamma_1-\gamma_2}{2}$ are the differences between the resonance frequencies and loss rates. Generally, the coupling strength g can be adjusted by the distance between the GNR and WSe_2, while ω_{diff} and γ_{diff} can be adjusted by the geometric size of the GNR. The complex eigenvalues of the hybrid system will coalesce when $\sqrt{g^2 + (\omega_{\mathrm{diff}} + i\gamma_{\mathrm{diff}})^2} = 0$, and an EP can be achieved.

We use the scattering spectrum, which is experimentally accessible, to extract the resonance frequencies and loss rates of the hybrid modes. A typical scattering spectrum of the plasmon-exciton system is shown in Fig. 1(b). The scattering spectrum can be calculated by standard finite-difference time-domain (FDTD) simulation. By fitting the scattering spectrum with a double-Lorentzian function, we can obtain the resonance frequencies and loss rates of the hybrid modes, as shown in Fig. 1(b), which correspond to the real and imaginary parts of the eigenvalues of the system.

The coupling strength between the GNR and WSe_2 is usually hard to precisely control in the experiment due to the nanoscale interaction length [59]. In order to overcome this difficulty, we propose to use the auxiliary layer of HfO_2, the thickness of which can be accurately controlled with current experimental technology; e.g., atomic layer deposition equipment can be used to deposit a layer of HfO_2 over WSe_2 with nanometer resolution. Then, the GNR can be transferred onto the sample by spin coating in order to obtain the device depicted in Fig. 1(a), similar to the sample preparation in Ref. [59]. By adjusting the thickness of the auxiliary layer of HfO_2, we can tune the coupling strength precisely between GNR and WSe_2. Figure 1(c) shows typical scattering spectra

for various thicknesses of the HfO_2 layer. Another physical parameter we control is the intrinsic resonance frequency of the GNR. It is tunable by adjusting the length of the GNR. Figure 1(d) shows the scattering spectra for various lengths of GNR in the hybrid system.

3. RESULTS

The precise control over the coupling strength and relative resonance frequencies allows us to realize and observe the EP in the plasmon-exciton system. Figure 2(a) depicts the cross section view of the system. We tune the thickness of the HfO_2 layer from 12 to 28 nm and the length of the GNR from 90 to 100 nm. For each choice of HfO_2 thickness and GNR length, we numerically simulate the scattering spectrum of the system. Then, as described earlier, we fit each scattering spectrum to obtain the resonance frequencies and loss rates of the two hybrid modes, which correspond to the real and imaginary parts of the eigenspectrum of the hybrid system. Plotting the resonance frequencies and loss rates of the hybrid modes as a function of HfO_2 thickness and GNR length, we obtain the eigenspectrum of the system. We can observe an EP at HfO_2 thickness ≈20 nm and GNR length ≈93.6 nm, where both the resonance frequencies and loss rates coalesce, as shown in Figs. 2(b) and 2(c). The eigenspectrum has the same topology as the Riemann surface of the complex function $f(z) = \sqrt{z}$. We also considered configuration II depicted in Fig. 2(d), where the GNR is placed directly on top of the glass substrate, parallel to the edge of the WSe_2 monolayer. The distance between GNR and WSe_2 tunes the coupling strength between plasmon and exciton modes. We plot the eigenspectrum of the hybrid system in the parameter space of GNR length and distance between GNR and WSe_2, and we observe an EP at a distance ≈14 nm with GNR length ≈107.6 nm, as shown in Figs. 2(e) and 2(f). However, as this configuration requires more delicate experimental control techniques, we will use configuration I in Fig. 2(a) for the sensing application.

As we have observed the EP in the plasmon-exciton system, we continue to explore its application in EP-enhanced sensing. We first consider the sensing of environmental refractive index, which is essential for environmental monitoring and chemical sensing. Variation in the refractive index leads to the variation of the resonance frequency of the GNR, and this effect can be enhanced by the EP in the hybrid system. In order to simulate the sensing of the environmental refractive index, we add a cladding layer with a variable refractive index on top of the plasmon-exciton hybrid sensor. In Fig. 3, we compare the sensitivity of EP-enhanced sensing using a plasmon-exciton hybrid sensor (performed near the EP with HfO_2 thickness = 20 nm and GNR length = 93.6 nm) and regular sensing using a GNR-only sensor. In Figs. 3(a) and 3(b), we show the scattering spectra of EP-enhanced sensing and regular sensing for various refractive indices. In Fig. 3(c), we show the variation of resonance frequency difference $[\Delta\omega = \Delta(\omega_1 - \omega_2)]$ and loss rate difference $[\Delta\gamma = \Delta(\gamma_1 - \gamma_2)]$ between the hybrid modes of the plasmon-exciton sensor, as well as the variation of resonance

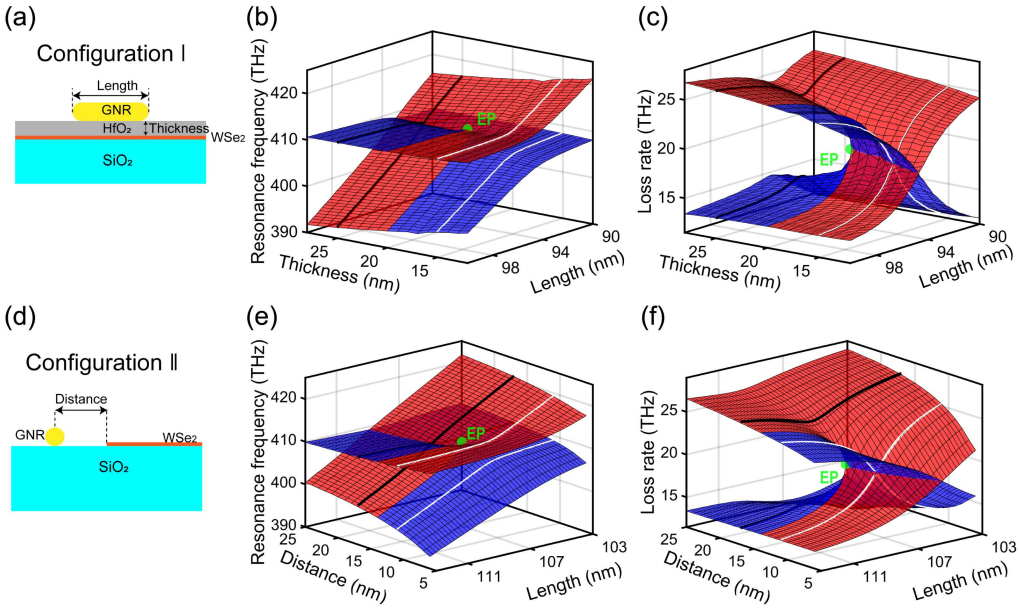

Fig. 2. Spectra and EPs of plasmon-exciton systems. (a) Plasmon-exciton system of configuration I, where GNR and WSe_2 are separated by an auxiliary layer of HfO_2. (b), (c) Resonance frequencies and loss rates of the plasmon-exciton system of configuration I, which correspond to the real and imaginary parts of the eigenspectrum of the hybrid system. The length of GNR and the thickness of HfO_2 are the control parameters. An EP (green dot) is observed when WSe_2 thickness ≈20 nm and GNR length ≈93.6 nm. The black and white lines correspond to a strong coupling regime (with avoided frequency crossing) and a weak coupling regime (with frequency crossing). (d) Plasmon-exciton system of configuration II, where GNR and WSe_2 are placed directly on top of the SiO_2 substrate. (e), (f) Resonance frequencies and loss rates of the plasmon-exciton system of configuration II, which correspond to the real and imaginary parts of the eigenspectrum of the hybrid system. The length of GNR and the distance between GNR and WSe_2 are the control parameters. An EP (green dot) is observed when the distance ≈14 nm and GNR length ≈107.6 nm. The white and black lines correspond to a strong coupling regime (with avoided frequency crossing) and a weak coupling regime (with frequency crossing). Each grid point corresponds to a data point from numerical simulation. The grid lines and surface coloring are guides to the eye.

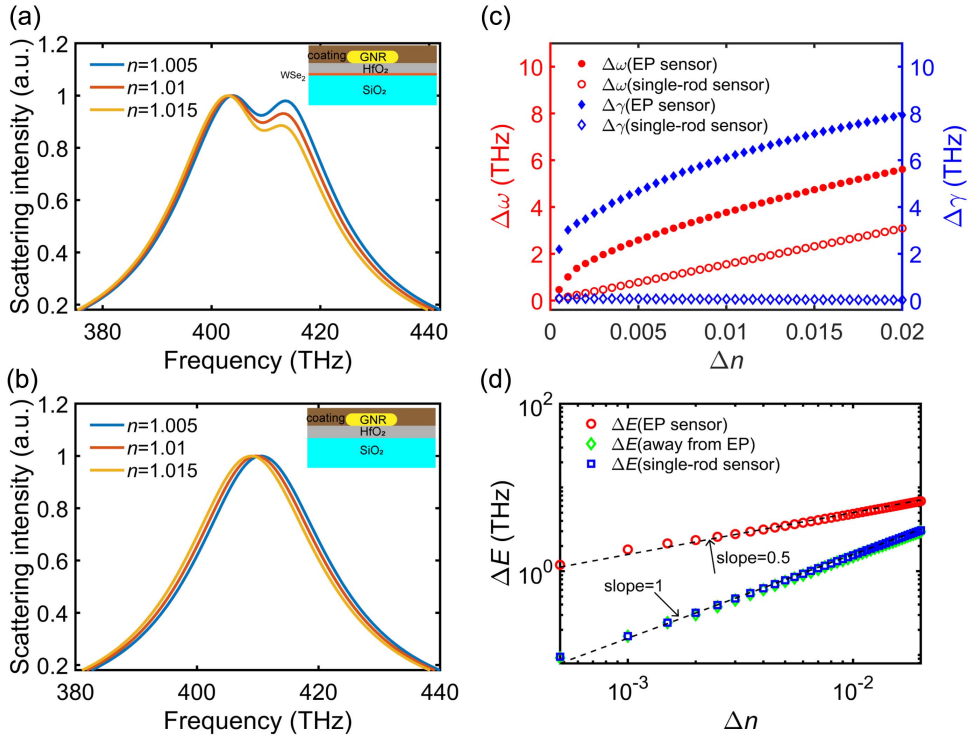

Fig. 3. Sensing of environmental refractive index with a plasmon-exciton sensor. (a) Scattering spectra of EP-enhanced sensing of environmental refractive index with a plasmon-exciton sensor. The system is covered by a cladding layer with a refractive index of $n = 1.005$, 1.01, or 1.015 to simulate the environmental refractive index change. The sensing is performed near the EP (with HfO_2 thickness = 20 nm and GNR length = 93.6 nm). (b) Scattering spectra of regular sensing with a GNR-only sensor (HfO_2 thickness = 20 nm and GNR length = 93.6 nm). The configuration is similar to that in (a) for comparison but without the WSe_2 monolayer. There is no EP in this system. (c) Variation of resonance frequency difference [$\Delta\omega = \Delta(\omega_1 - \omega_2)$] and loss rate difference [$\Delta\gamma = \Delta(\gamma_1 - \gamma_2)$] between the hybrid modes of the plasmon-exciton sensor and variation of resonance frequency and loss rate of the GNR-only sensor in response to environmental refractive index change. (d) Absolute value variation of the eigenvalue difference [$\Delta E = \sqrt{(\Delta\omega)^2 + (\Delta\gamma/2)^2}$] between the hybrid modes of the plasmon-exciton sensor near the EP and absolute value variation of the eigenvalue of the GNR-only sensor in response to environmental refractive index change. The EP-enhanced plasmon-exciton sensor is more sensitive to the variation of the refractive index and follows the square root signature near the EP, while the regular GNR-only sensor is less sensitive and follows a linear trend. For comparison, we also plot the absolute value variation of the eigenvalue difference of a plasmon-exciton sensor (with HfO_2 thickness = 25 nm and GNR length = 100 nm) as a function of the environmental refractive index change. It shows a linear behavior similar to the regular GNR-only sensor, as the parameters are set far away from the EP.

frequency and loss rate of the GNR-only sensor, in response to the environmental refractive index change. Figure 3(d) shows the absolute value variation of the eigenvalue difference [$\Delta E = \sqrt{(\Delta\omega)^2 + (\Delta\gamma/2)^2}$] between the hybrid modes of the plasmon-exciton sensor and also the absolute value variation of the eigenvalue of the GNR-only sensor in response to the environmental refractive index change. As we can see from Fig. 3(d), the EP-enhanced plasmon-exciton sensor is more sensitive to environmental refractive index perturbation than the regular GNR-only sensor. The EP-enhanced sensing follows the square root signature near the EP with higher sensitivity, while regular sensing follows a linear trend with less sensitivity. The sensitivity factor of the regular GNR-only sensor is on the order of 100 THz per unit change of refractive index, which is consistent with earlier works [63,64], while the sensitivity factor of the EP-enhanced sensor can be more than 10 fold higher, depending on how close the sensor is to the EP. With an experimentally achievable resolution of 1 THz, the regular GNR-only sensor can detect a refractive index change on the order of 0.01, while the EP-enhanced sensor can detect a refractive index change on the order of 0.001. For comparison purposes, we also plot the sensing with a plasmon-exciton sensor whose parameters are set far away from the EP, and it shows a linear behavior similar to the regular GNR-only sensor without EP enhancement.

In addition to the EP-enhanced sensitivity, the plasmon-exciton hybrid sensor has the capability of nanoscale sensing for the environmental refractive index due to the sub-diffraction-limit size of the plasmonic resonator. We simulate the nanoscale sensing by a local refractive index variation within a box region (200 nm × 100 nm × 100 nm) surrounding the GNR, as shown in Fig. 4(a), instead of a homogenous refractive index variation, as discussed earlier in Fig. 3. We numerically calculate the absolute value variation of the eigenvalue difference [$\Delta E = \sqrt{(\Delta\omega)^2 + (\Delta\gamma/2)^2}$] between the hybrid modes of the plasmon-exciton sensor for both the nanoscale refractive index variation [green crosses in Fig. 4(b)] and the homogenous refractive index variation [red circles in Fig. 4(b) for comparison, the same as red circles in Fig. 3(d)]. We can see that the sensitivity of the EP-enhanced sensor for nanoscale refractive

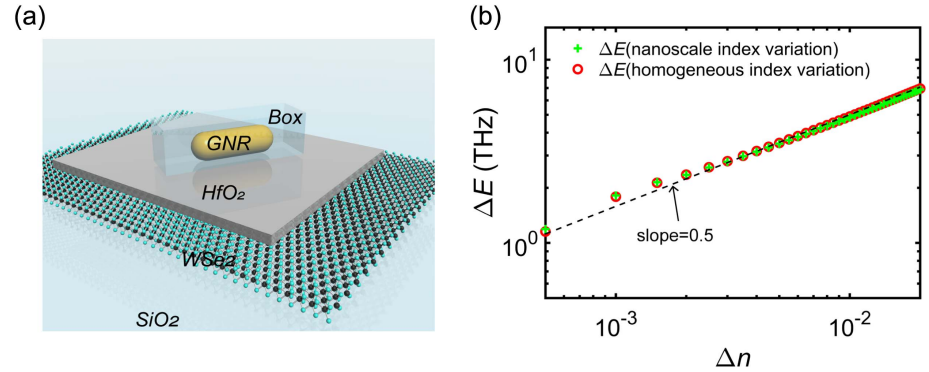

Fig. 4. Nanoscale sensing of environmental refractive index with a plasmon-exciton sensor. (a) Schematic of nanoscale sensing of the environmental refractive index variation within the box region (200 nm × 100 nm × 100 nm) surrounding the GNR. (b) Absolute value variation of the eigenvalue difference $[\Delta E = \sqrt{(\Delta\omega)^2 + (\Delta\gamma/2)^2}]$ between the hybrid modes of the plasmon-exciton sensor in response to environmental refractive index change. The sensitivity of the EP-enhanced plasmon-exciton sensor for nanoscale refractive index variation (green) agrees well with that for homogeneous environmental refractive index variation (red), showing the square root signature near the EP.

index variation agrees well with that for homogeneous environmental refractive index variation. This shows the nanoscale EP-enhanced sensing capability of the plasmon-exciton hybrid sensor.

The EP-enhanced sensor can also be used for nanoparticle sensing. For example, it can be used to check the length of a GNR in a non-invasive way. In this case, the GNR is both part of the plasmon-exciton hybrid system and the object to be measured. In Figs. 5(a) and 5(b), we show the scattering spectra of EP-enhanced sensing with plasmon-exciton hybrid modes and regular sensing with a single plasmonic mode for various GNR lengths. In Fig. 5(c), we show the variation of resonance

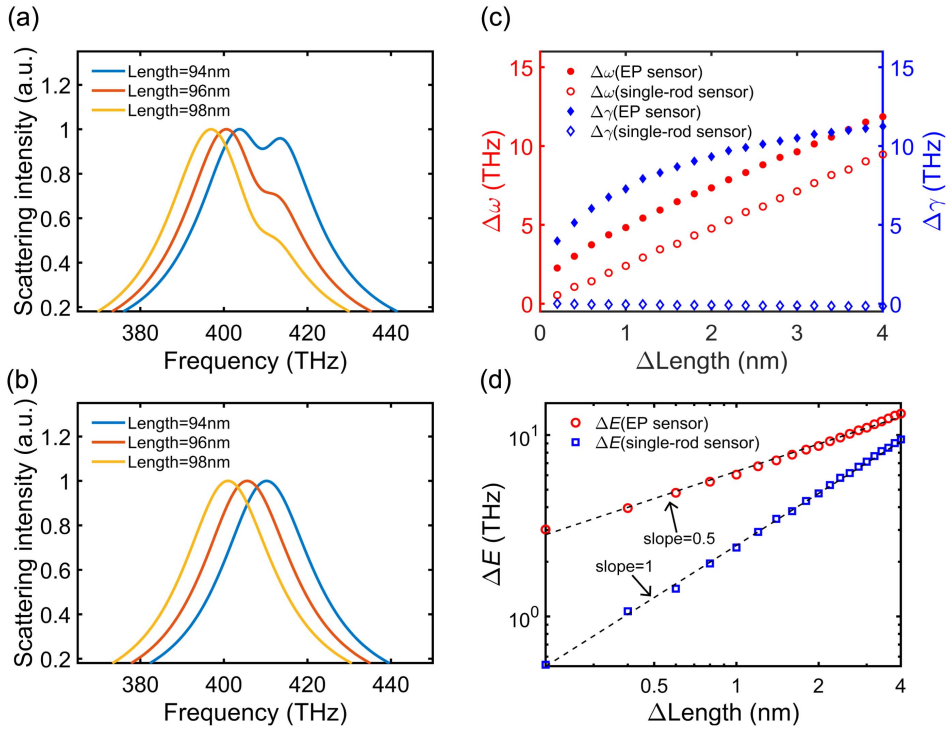

Fig. 5. Sensing of nanoparticle length. (a) Scattering spectra of EP-enhanced sensing of GNR length by plasmon-exciton hybridization. The GNR can be randomly placed on top of the sensor within the area of WSe_2 to form a hybrid system. (b) Scattering spectra of regular sensing of a GNR. The configuration is similar to that in (a) for comparison, but without the WSe_2 monolayer. There is no EP in this case. (c) Variation of resonance frequency difference and loss rate difference between the hybrid modes and variation of resonance frequency and loss rate of the single plasmonic mode in response to GNR length change. (d) Absolute value variation of the eigenvalue difference between the hybrid modes and absolute value variation of the eigenvalue of the single plasmonic mode in response to GNR length change. The EP-enhanced sensing with plasmon-exciton hybridization is more sensitive to nanoscale change in the GNR length and follows the square root signature near the EP, while regular sensing is less sensitive and follows a linear trend.

frequency difference and loss rate difference between the hybrid modes and variation of resonance frequency and loss rate of the single plasmonic mode as the GNR length changes. In Fig. 5(d), we compare the absolute value variation of the eigenvalue difference between the hybrid modes and the absolute value variation of the eigenvalue of the single plasmonic mode. Again, we see that the EP-enhanced sensing with plasmon-exciton hybridization is more sensitive and follows the square root signature near the EP.

4. CONCLUSION

In conclusion, EPs are realized in plasmon-exciton hybrid systems. Plasmon-exciton sensors with EP-enhanced sensitivity can be used for nanoscale sensing of environmental refractive index changes and nanoparticles. They can also be used to detect other nanoparticles or materials that either change the effective refractive index around the GNR or modify the coupling between the plasmon and exciton modes and could find real-life applications such as environmental monitoring and biomolecule detection.

Funding. National Key Research and Development Program of China (2018YFB2200401); National Natural Science Foundation of China (11527901, 11974031, 12174009, 61521004, 91950111).

Disclosures. The authors declare no conflicts of interest.

Data Availability. Data underlying the results presented in this paper are not publicly available at this time but may be obtained from the authors upon reasonable request.

REFERENCES

1. D. Heiss, "Circling exceptional points," Nat. Phys. **12**, 823–824 (2016).
2. R. El-Ganainy, K. G. Makris, M. Khajavikhan, Z. H. Musslimani, S. Rotter, and D. N. Christodoulides, "Non-Hermitian physics and PT symmetry," Nat. Phys. **14**, 11–19 (2018).
3. M. A. Miri and A. Alu, "Exceptional points in optics and photonics," Science **363**, eaar7709 (2019).
4. S. K. Ozdemir, S. Rotter, F. Nori, and L. Yang, "Parity-time symmetry and exceptional points in photonics," Nat. Mater. **18**, 783–798 (2019).
5. T. Kato, *Perturbation Theory of Linear Operators* (Springer, 1966).
6. C. Dembowski, H. Graf, H. L. Harney, A. Heine, W. D. Heiss, H. Rehfeld, and A. Richter, "Experimental observation of the topological structure of exceptional points," Phys. Rev. Lett. **86**, 787–790 (2001).
7. S. Bittner, B. Dietz, U. Gunther, H. L. Harney, M. Miski-Oglu, A. Richter, and F. Schafer, "PT symmetry and spontaneous symmetry breaking in a microwave billiard," Phys. Rev. Lett. **108**, 024101 (2012).
8. A. Guo, G. J. Salamo, D. Duchesne, R. Morandotti, M. Volatier-Ravat, V. Aimez, G. A. Siviloglou, and D. N. Christodoulides, "Observation of PT-symmetry breaking in complex optical potentials," Phys. Rev. Lett. **103**, 093902 (2009).
9. S. B. Lee, J. Yang, S. Moon, S. Y. Lee, J. B. Shim, S. W. Kim, J. H. Lee, and K. An, "Observation of an exceptional point in a chaotic optical microcavity," Phys. Rev. Lett. **103**, 134101 (2009).
10. M. Brandstetter, M. Liertzer, C. Deutsch, P. Klang, J. Schoberl, H. E. Tureci, G. Strasser, K. Unterrainer, and S. Rotter, "Reversing the pump dependence of a laser at an exceptional point," Nat. Commun. **5**, 4034 (2014).
11. B. Zhen, C. W. Hsu, Y. Igarashi, L. Lu, I. Kaminer, A. Pick, S. L. Chua, J. D. Joannopoulos, and M. Soljacic, "Spawning rings of exceptional points out of Dirac cones," Nature **525**, 354–358 (2015).
12. Z. Lin, A. Pick, M. Loncar, and A. W. Rodriguez, "Enhanced spontaneous emission at third-order Dirac exceptional points in inverse-designed photonic crystals," Phys. Rev. Lett. **117**, 107402 (2016).
13. W. Chen, S. Kaya Ozdemir, G. Zhao, J. Wiersig, and L. Yang, "Exceptional points enhance sensing in an optical microcavity," Nature **548**, 192–196 (2017).
14. H. Hodaei, A. U. Hassan, S. Wittek, H. Garcia-Gracia, R. El-Ganainy, D. N. Christodoulides, and M. Khajavikhan, "Enhanced sensitivity at higher-order exceptional points," Nature **548**, 187–191 (2017).
15. T. Goldzak, A. A. Mailybaev, and N. Moiseyev, "Light stops at exceptional points," Phys. Rev. Lett. **120**, 013901 (2018).
16. H. Zhou, C. Peng, Y. Yoon, C. W. Hsu, K. A. Nelson, L. Fu, J. D. Joannopoulos, M. Soljacic, and B. Zhen, "Observation of bulk Fermi arc and polarization half charge from paired exceptional points," Science **359**, 1009–1012 (2018).
17. H. Zhao, Z. Chen, R. Zhao, and L. Feng, "Exceptional point engineered glass slide for microscopic thermal mapping," Nat. Commun. **9**, 1764 (2018).
18. S. Wang, B. Hou, W. Lu, Y. Chen, Z. Q. Zhang, and C. T. Chan, "Arbitrary order exceptional point induced by photonic spin-orbit interaction in coupled resonators," Nat. Commun. **10**, 832 (2019).
19. M. A. Quiroz-Juárez, A. Perez-Leija, K. Tschernig, B. M. Rodríguez-Lara, O. S. Magaña-Loaiza, K. Busch, Y. N. Joglekar, and R. D. J. León-Montiel, "Exceptional points of any order in a single, lossy waveguide beam splitter by photon-number-resolved detection," Photon. Res. **7**, 862–867 (2019).
20. J. H. Park, A. Ndao, W. Cai, L. Y. Hsu, A. Kodigala, T. Lepetit, Y. H. Lo, and B. Kante, "Symmetry-breaking-induced plasmonic exceptional points and nanoscale sensing," Nat. Phys. **16**, 462–468 (2020).
21. C. Q. Wang, X. F. Jiang, G. M. Zhao, M. Z. Zhang, C. W. Hsu, B. Peng, A. D. Stone, L. Jiang, and L. Yang, "Electromagnetically induced transparency at a chiral exceptional point," Nat. Phys. **16**, 334–340 (2020).
22. T. Wu, W. Zhang, H. Zhang, S. Hou, G. Chen, R. Liu, C. Lu, J. Li, R. Wang, P. Duan, J. Li, B. Wang, L. Shi, J. Zi, and X. Zhang, "Vector exceptional points with strong superchiral fields," Phys. Rev. Lett. **124**, 083901 (2020).
23. A. Bergman, R. Duggan, K. Sharma, M. Tur, A. Zadok, and A. Alu, "Observation of anti-parity-time-symmetry, phase transitions and exceptional points in an optical fibre," Nat. Commun. **12**, 486 (2021).
24. L. Xiao, T. Deng, K. Wang, Z. Wang, W. Yi, and P. Xue, "Observation of non-Bloch parity-time symmetry and exceptional points," Phys. Rev. Lett. **126**, 230402 (2021).
25. W. Zhang, H. Chiang, T. Wen, L. Ye, H. Lin, H. Xu, Q. Gong, and G. Lu, "Exotic coupling between plasmonic nanoparticles through geometric configurations," J. Lightwave Technol. **39**, 6646–6652 (2021).
26. C. Wang, W. R. Sweeney, A. D. Stone, and L. Yang, "Coherent perfect absorption at an exceptional point," Science **373**, 1261–1265 (2021).
27. G. Q. Qin, R. R. Xie, H. Zhang, Y. Q. Hu, M. Wang, G. Q. Li, H. T. Xu, F. C. Lei, D. Ruan, and G. L. Long, "Experimental realization of sensitivity enhancement and suppression with exceptional surfaces," Laser Photon. Rev. **15**, 2000569 (2021).
28. H. Xu, D. Mason, L. Jiang, and J. G. Harris, "Topological energy transfer in an optomechanical system with exceptional points," Nature **537**, 80–83 (2016).
29. J. Zhang, B. Peng, S. K. Ozdemir, K. Pichler, D. O. Krimer, G. M. Zhao, F. Nori, Y. X. Liu, S. Rotter, and L. Yang, "A phonon laser operating at an exceptional point," Nat. Photonics **12**, 479–484 (2018).
30. Y. Choi, S. Kang, S. Lim, W. Kim, J. R. Kim, J. H. Lee, and K. An, "Quasieigenstate coalescence in an atom-cavity quantum composite," Phys. Rev. Lett. **104**, 153601 (2010).
31. L. Ding, K. Shi, Q. Zhang, D. Shen, X. Zhang, and W. Zhang, "Experimental determination of PT-symmetric exceptional points in a single trapped ion," Phys. Rev. Lett. **126**, 083604 (2021).
32. T. Stehmann, W. D. Heiss, and F. G. Scholtz, "Observation of exceptional points in electronic circuits," J. Phys. A **37**, 7813–7819 (2004).
33. M. Sakhdari, M. Hajizadegan, Q. Zhong, D. N. Christodoulides, R. El-Ganainy, and P. Y. Chen, "Experimental observation of PT symmetry breaking near divergent exceptional points," Phys. Rev. Lett. **123**, 193901 (2019).

34. L. J. Fernandez-Alcazar, H. Li, F. Ellis, A. Alu, and T. Kottos, "Robust scattered fields from adiabatically driven targets around exceptional points," Phys. Rev. Lett. **124**, 133905 (2020).
35. Z. Guo, T. Zhang, J. Song, H. Jiang, and H. Chen, "Sensitivity of topological edge states in a non-Hermitian dimer chain," Photon. Res. **9**, 574–582 (2021).
36. S. Yao and Z. Wang, "Edge states and topological invariants of non-Hermitian systems," Phys. Rev. Lett. **121**, 086803 (2018).
37. K. Kawabata, T. Bessho, and M. Sato, "Classification of exceptional points and non-Hermitian topological semimetals," Phys. Rev. Lett. **123**, 066405 (2019).
38. W. Tang, X. Jiang, K. Ding, Y. X. Xiao, Z. Q. Zhang, C. T. Chan, and G. Ma, "Exceptional nexus with a hybrid topological invariant," Science **370**, 1077–1080 (2020).
39. T. Gao, E. Estrecho, K. Y. Bliokh, T. C. Liew, M. D. Fraser, S. Brodbeck, M. Kamp, C. Schneider, S. Hofling, Y. Yamamoto, F. Nori, Y. S. Kivshar, A. G. Truscott, R. G. Dall, and E. A. Ostrovskaya, "Observation of non-Hermitian degeneracies in a chaotic exciton-polariton billiard," Nature **526**, 554–558 (2015).
40. D. Zhang, X. Q. Luo, Y. P. Wang, T. F. Li, and J. Q. You, "Observation of the exceptional point in cavity magnon-polaritons," Nat. Commun. **8**, 1368 (2017).
41. A. Ben-Asher, D. Simsa, T. Uhlirova, M. Sindelka, and N. Moiseyev, "Laser control of resonance tunneling via an exceptional point," Phys. Rev. Lett. **124**, 253202 (2020).
42. W. D. Heiss, "Phases of wave functions and level repulsion," Eur. Phys. J. D **7**, 1–4 (1999).
43. M. V. Berry, "Physics of nonhermitian degeneracies," Czech. J. Phys. **54**, 1039–1047 (2004).
44. R. Lefebvre, O. Atabek, M. Sindelka, and N. Moiseyev, "Resonance coalescence in molecular photodissociation," Phys. Rev. Lett. **103**, 123003 (2009).
45. R. Uzdin, A. Mailybaev, and N. Moiseyev, "On the observability and asymmetry of adiabatic state flips generated by exceptional points," J. Phys. A **44**, 435302 (2011).
46. S. W. Kim, "Braid operation of exceptional points," Fortschr. Phys. **61**, 155–161 (2013).
47. P. R. Kapralova-Zdanska and N. Moiseyev, "Helium in chirped laser fields as a time-asymmetric atomic switch," J. Chem. Phys. **141**, 014307 (2014).
48. M. Hamamda, P. Pillet, H. Lignier, and D. Comparat, "Ro-vibrational cooling of molecules and prospects," J. Phys. B **48**, 182001 (2015).
49. T. J. Milburn, J. Doppler, C. A. Holmes, S. Portolan, S. Rotter, and P. Rabl, "General description of quasiadiabatic dynamical phenomena near exceptional points," Phys. Rev. A **92**, 052124 (2015).
50. A. U. Hassan, B. Zhen, M. Soljacic, M. Khajavikhan, and D. N. Christodoulides, "Dynamically encircling exceptional points: exact evolution and polarization state conversion," Phys. Rev. Lett. **118**, 093002 (2017).
51. H. Xu, D. Mason, and L. Jiang, "Topological dynamics in an optomechanical system with highly non-degenerate modes," arXiv: 1703.07374 (2017).
52. J. Doppler, A. A. Mailybaev, J. Bohm, U. Kuhl, A. Girschik, F. Libisch, T. J. Milburn, P. Rabl, N. Moiseyev, and S. Rotter, "Dynamically encircling an exceptional point for asymmetric mode switching," Nature **537**, 76–79 (2016).
53. Y. Choi, C. Hahn, J. W. Yoon, S. H. Song, and P. Berini, "Extremely broadband, on-chip optical nonreciprocity enabled by mimicking nonlinear anti-adiabatic quantum jumps near exceptional points," Nat. Commun. **8**, 14154 (2017).
54. J. W. Yoon, Y. Choi, C. Hahn, G. Kim, S. H. Song, K. Y. Yang, J. Y. Lee, Y. Kim, C. S. Lee, J. K. Shin, H. S. Lee, and P. Berini, "Time-asymmetric loop around an exceptional point over the full optical communications band," Nature **562**, 86–90 (2018).
55. X. L. Zhang, T. Jiang, and C. T. Chan, "Dynamically encircling an exceptional point in anti-parity-time symmetric systems: asymmetric mode switching for symmetry-broken modes," Light Sci. Appl. **8**, 88 (2019).
56. A. Li, J. Dong, J. Wang, Z. Cheng, J. S. Ho, D. Zhang, J. Wen, X. L. Zhang, C. T. Chan, A. Alu, C. W. Qiu, and L. Chen, "Hamiltonian hopping for efficient chiral mode switching in encircling exceptional points," Phys. Rev. Lett. **125**, 187403 (2020).
57. Q. Liu, S. Li, B. Wang, S. Ke, C. Qin, K. Wang, W. Liu, D. Gao, P. Berini, and P. Lu, "Efficient mode transfer on a compact silicon chip by encircling moving exceptional points," Phys. Rev. Lett. **124**, 153903 (2020).
58. M. Zhang, W. Sweeney, C. W. Hsu, L. Yang, A. D. Stone, and L. Jiang, "Quantum noise theory of exceptional point amplifying sensors," Phys. Rev. Lett. **123**, 180501 (2019).
59. A. Hu, W. Zhang, S. Liu, T. Wen, J. Zhao, Q. Gong, Y. Ye, and G. Lu, "*In situ* scattering of single gold nanorod coupling with monolayer transition metal dichalcogenides," Nanoscale **11**, 20734–20740 (2019).
60. J. Sun, H. Hu, D. Zheng, D. Zhang, Q. Deng, S. Zhang, and H. Xu, "Light-emitting plexciton: exploiting plasmon–exciton interaction in the intermediate coupling regime," ACS Nano **12**, 10393–10402 (2018).
61. X. Li, L. Zhou, Z. Hao, and Q.-Q. Wang, "Plasmon-exciton coupling in complex systems," Adv. Opt. Mater. **6**, 1800275 (2018).
62. S. N. Gupta, O. Bitton, T. Neuman, R. Esteban, L. Chuntonov, J. Aizpurua, and G. Haran, "Complex plasmon-exciton dynamics revealed through quantum dot light emission in a nanocavity," Nat. Commun. **12**, 1310 (2021).
63. M. H. Elshorbagy, A. Cuadrado, and J. Alda, "Plasmonic sensor based on dielectric nanoprisms," Nano. Res. Lett. **12**, 580 (2017).
64. G. Lu, L. Hou, T. Zhang, J. Liu, H. Shen, C. Luo, and Q. Gong, "Plasmonic sensing via photoluminescence of individual gold nanorod," J. Phys. Chem. C **116**, 25509–25516 (2012).